Real-Time Visualization of Assembling of a Sphingomyelin-Specific Toxin on Planar Lipid Membranes

Neval Yilmaz,[†] Taro Yamada,[†] Peter Greimel,[†] Takayuki Uchihashi,[‡§] Toshio Ando,[‡§] and Toshihide Kobayashi[†¶*]
[†]Lipid Biology Laboratory, RIKEN, Wako, Saitama, Japan; [‡]Department of Physics and [§]Bio-AFM Frontier Research Center, Kanazawa University, Kanazawa, Ishikawa, Japan; and [¶]Institut National de la Santé et de la Recherche Médicale U1060-Université Lyon 1, Villeurbanne, France

ABSTRACT Pore-forming toxins (PFTs) are soluble proteins that can oligomerize on the cell membrane and induce cell death by membrane insertion. PFT oligomers sometimes form hexagonal close-packed (hcp) structures on the membrane. Here, we show the assembling of the sphingomyelin (SM)-binding PFT, lysenin, into an hcp structure after oligomerization on SM/cholesterol membrane. This process was monitored by high-speed atomic force microscopy. Hcp assembly was driven by reorganization of lysenin oligomers such as association/dissociation and rapid diffusion along the membrane. Besides rapid association/dissociation of oligomers, the height change for some oligomers, possibly resulting from conformational changes in lysenin, could also be visualized. After the entire membrane surface was covered with a well-ordered oligomer lattice, the lysenin molecules were firmly bound on the membrane and the oligomers neither dissociated nor diffused. Our results reveal the dynamic nature of the oligomers of a lipid-binding toxin during the formation of an hcp structure. Visualization of this dynamic process is essential for the elucidation of the assembling mechanism of some PFTs that can form ordered structures on the membrane.

INTRODUCTION

Pore-forming toxins (PFTs) are soluble proteins found in a wide spectrum of organisms, including bacteria, fungi, and animals, and they exert toxic effects by binding the target membranes, where they assemble into oligomers (1). PFT oligomers are sometimes organized into two-dimensional hexagonal close-packed (hcp) structures that have been resolved by electron and atomic force microscopy in model membranes (2–4). The mechanism of the formation of hcp structures on lipid membranes is of interest, because oligomer formation can occur randomly on the membrane.

In this study, we focused on the assembly of the earthworm-derived 297-aa-long pore-forming toxin, lysenin (5,6). Lysenin is known for its specific interaction with sphingomyelin (SM) (7,8). Recently, the crystal structure of lysenin revealed the presence of multiple SM binding sites (9). SM is one of the major lipids in the outer leaflet of the plasma membrane of mammalian cells. SM is a reservoir of the signaling lipid, ceramide (10). It also forms lipid domains with cholesterol (chol) known as "lipid rafts" (11). The specific interaction between SM and lysenin enables the detection of SM, and hence, allows the examination of the lipid distribution within the membrane (12,13). By transmission electron microscopy, it was revealed that lysenin oligomerizes and forms hcp structures on liposomes of SM and chol (8). Although lysenin oligomerizes only in the presence of SM, chol is essential for the formation of an hcp structure, as it facilitates the oligomerization of lysenin (14).

Here, we report the spatiotemporal dynamics of lysenin oligomers during their assembling on the SM/chol bilayer. To monitor this process, we utilized high-speed atomic force microscopy (HS-AFM). HS-AFM, which was recently developed (15), has enabled the real-time imaging of the dynamics of some membrane proteins at subsecond resolution (16–18). By using this state of the art technique for a pore-forming toxin, we revealed (to our knowledge, for the first time) the mechanism of the formation of an hcp structure, which involves cooperative association/dissociation (i.e., the simultaneous association or dissociation of several oligomers) and lateral diffusion of the toxin along the membrane surface in milliseconds.

MATERIALS AND METHODS

Materials

Lysenin from earthworm, *Eisenia foetida*, was obtained from Peptide Institute (Osaka, Japan). Brain SM and chol (≥99%) were purchased from Avanti Polar Lipids (Alabama, AL) and Sigma (St. Louis, MO), respectively. Multilamellar vesicles (MLVs) of SM and SM/chol (1:1) were prepared from a homogeneous lipid mixture in chloroform. The thin lipid film formed after evaporation of chloroform was hydrated with a solution of phosphate-buffered saline (PBS, 10 mM, pH = 7.5; Sigma) to a total lipid concentration of 1 mM by heating to 55°C and vortex mixing. The lipid suspensions were additionally sonicated in a bath sonicator at 38 kHz. The sonication duration was 10 min for SM suspension and 5 min for SM/chol suspension. The obtained MLVs were frozen at −80°C and thawed at 55°C twice. Unilamellar vesicles were prepared by sonication of MLVs at 20 kHz with an ultrasonic homogenizer, UH-50 from SMT (Tokyo, Japan), for 10 min. The vesicle size was measured by dynamic light scattering using a Zetasizer Nano ZS (Malvern, Worcestershire, UK). The size of the vesicles was found to be ~120 nm (see Fig. S1 in the Supporting Material). Lysenin was dissolved in PBS to a final concentration of 15 μM.

Submitted April 2, 2013, and accepted for publication July 22, 2013.

*Correspondence: kobayasi@riken.jp

Editor: Simon Scheuring.

0006-3495/13/09/1397/9 $2.00

http://dx.doi.org/10.1016/j.bpj.2013.07.052

Visualization of lysenin oligomers on lipid bilayer

High-speed atomic force microscopy (HS-AFM) measurements to visualize lysenin binding and assembling on SM-containing bilayer were performed at Kanazawa University and also in part at Research Institute of Biomolecule Metrology (RIBM, Tsukuba, Japan) using the Nanoexplorer and Nano Live Vision systems (RIBM). A sample stage made of quartz was placed on the Z-scanner. A mica disk with a diameter of 1.5 mm was glued onto the sample stage. A detailed report by Uchihashi et al. (19) on HS-AFM setup is available. To prepare lipid bilayers, 1.5 μL of multilamellar or unilamellar vesicle suspension was dropped onto the mica disk and incubated for 5 min at 55°C. Mica surface was rinsed with pure water and placed onto the scanner. The surface was imaged in 70-μL PBS solution with cantilevers that had a resonant frequency of 500 kHz in water and a spring constant of 0.1 N/m. For in-situ measurements, AFM imaging was started just after introduction of lysenin diluted with a PBS solution to a concentration of 15 μM. At half-concentration, lysenin did not assemble into an hcp structure. This could be due to its slow diffusion from bulk solution to the vicinity of the membrane. The adsorption of lysenin on mica was visualized in situ at the same lysenin concentration, used for the observation of lysenin assembling on lipid bilayer. For preincubation experiments, 2 μL of diluted lysenin was dropped onto a mica-supported SM/chol bilayer and incubated for 15 min at room temperature. HS-AFM imaging was performed at room temperature.

Calculation of the average neighboring distance

We took the following processes to quantify the randomness of oligomer positions: To begin, we generated a table of *X-Y* coordinates of all oligomer centers in every AFM image, using a spot-readout software (GRAPHCEL, http://www9.plala.or.jp/kobo333/). Then, the two-dimensional plots of the oligomer positions were subjected to two-dimensional numerical Fourier transformation. The Fourier-transformed images are composed as the reciprocal-space lattice. This reciprocal lattice was converted to the real lattice. The real lattice exhibits hexagonal symmetry, and the real hexagonal lattice constant is hereafter designated as the average neighboring distance. The randomness (i.e., the average displacement of oligomers from the lattice points) was quantified by using the autocorrelation plots. The autocorrelation plots were obtained by calculating the two-dimensional displacement vectors of all the pairs of oligomers that appear in the image of oligomer *X-Y* coordinates. The autocorrelation plots, according to this definition, are significant only within the first nearest plots from the origin. Overlaying the two-dimensional real lattice (generated by the above-mentioned Fourier transformation) onto the autocorrelation plots within the first-nearest range, we can see that the autocorrelation plots are concentrated near the real lattice points. We calculated the distance between each autocorrelation plot and the real lattice point nearest to it, and the obtained distances were averaged over one frame. This average distance is the standard deviation, which indicates the randomness of oligomer positions in the frame.

Molecular modeling

The model of lysenin was based on Protein Data Bank entry PDB:3ZX7 (lysenin in complex with choline phosphate). The secondary structure of N-terminal residues 1–10 was predicted by the homology modeling and threading server I-TASSER without specified restraints (20–22), superimposed on N-terminal residues 5–10 of the x-ray structure and the four missing N-terminal residues 1–4 were manually connected to the Lysenin model. The protonation state of the resulting model was predicted utilizing the H++ server (23). The resulting model was parameterized utilizing the CHARMM C36 force field (24). The lysenin oligomers were assembled either utilizing pore-forming proteins featuring a central β-barrel structure of varying size as templates (e.g., PDB:1UYN, PDB:1PHO, PDB:3SZD) or manually. Subsequently, the oligomer assemblies were equilibrated for 1 ns at 310 K utilizing the NAMD 2.8 software package (25), before superimposition with AFM topology data utilizing custom-made VMD scripts (26).

Radial distribution function

The radial height distribution of stable hcp oligomers was established by mapping the relative brightness in the vicinity of lysenin oligomers. The ideal center of lysenin oligomers in the AFM images was determined via a custom-made computer script. Usual computational approaches based on particle identification procedures produced poor results due to the central cavity of lysenin oligomers. In total, the relative radial brightness distribution in the vicinity of ~900 lysenin oligomers was analyzed and averaged.

RESULTS AND DISCUSSION

Assembly of lysenin oligomers on SM/chol bilayer

Previously, using negative staining electron microscopy we revealed that lysenin oligomers assemble into an hcp structure when incubated with SM/chol liposomes (8). In this study, we preincubated SM/chol bilayer with lysenin (see Materials and Methods) before imaging by HS-AFM. Fig. 1, *A* and *B*, shows two- and three-dimensional images of the hcp arrangement of lysenin oligomers on the lipid bilayer. In Fig. 1 *A*, the hexagon that appears in open representation indicates a single hcp unit. The average neighboring distance in the hcp structure (i.e., the distance between the centers of two neighboring oligomers), estimated by two-dimensional Fourier transformation, was 13.1 $\pm$ 1.7 nm. The oligomers had an outer diameter of 10 nm with an inner pore of 5 nm, which was calculated using the radial distribution function (see Fig. S2). These values are in good agreement with the diameters of the lysenin oligomers and the pore-like structures on SM/chol liposomes, visualized by electron microscopy (8). In a recent study, the oligomeric assembly of lysenin was revealed by two-dimensional electron crystallography and the oligomer diameter was estimated to be 11.2 nm with an inner pore of 5.7 nm (9). The oligomeric assembly was considered to be a trimer or a hexamer. A hexamer can provide a sufficient number of β-strands to form membrane pores. The high similarity of our oligomer and pore diameters with De Colibus et al. (9) suggests the presence of comparable oligomerization state.

Whereas the oligomers of lysenin exhibit a uniform lateral size, the height profile revealed the presence of two distinct populations (Fig. 1 *B*). Due to the complete coverage of the observed membrane patches with lysenin oligomers, unambiguous determination of the oligomer height proofed to be challenging. To quantify the oligomer height, we assumed that the darkest areas represent the lipid bilayer. Based on this assumption, the height distribution in Fig. 1 *C* yielded two maxima: at 2.6 nm for the (darker) lower and 5 nm for the (brighter) taller oligomers, representing the majority of the population. The presence of lower-height

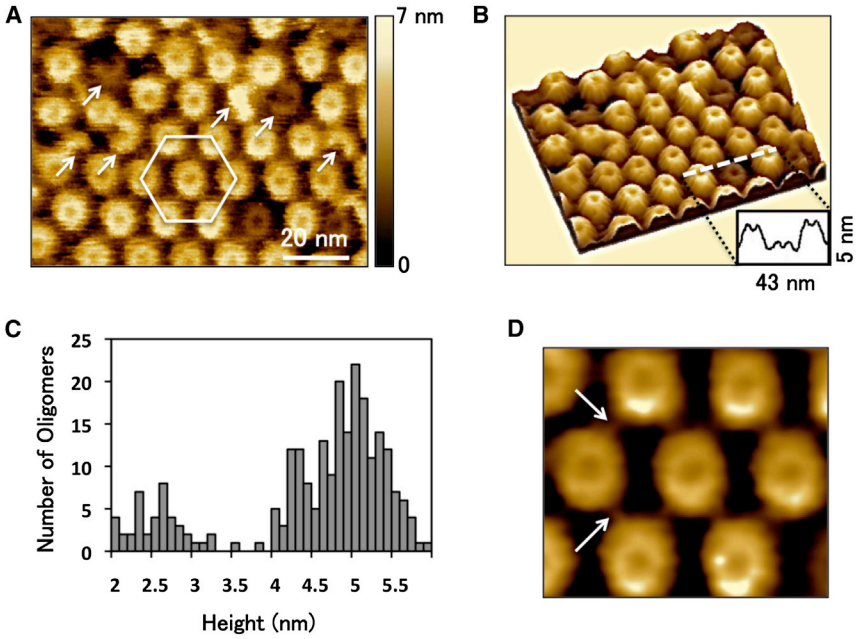

FIGURE 1 AFM images of hexagonal close-packed (hcp) assembly of lysenin oligomers on SM/chol (1:1) bilayer. Lysenin was preincubated with SM/chol (1:1) bilayer for 15 min and AFM imaging was performed in PBS at a scan rate of 0.5 frames/s. (*A*) Two-dimensional height image. (*B*) Three-dimensional height image. (*Inset*) Height analysis for the three adjacent oligomers (indicated by the *open dashed line*). (*C*) Histogram showing the height distribution for the (*dark*) lower and (*bright*) taller oligomers. (*D*) Enlarged band-pass filtered image of the hcp unit indicated by a hexagon in panel *A*. (*Arrows* in panels *A* and *D* show the incomplete oligomers and the linkages between oligomers, respectively.)

oligomers suggests the membrane insertion of lysenin. Previously, the oligomer height in the prepore and pore states of the cholesterol-binding cytolysin, perfringolysin O, was determined using AFM (27). It is thus possible that the taller oligomers are prepores and the lower ones are pores, although we cannot infer whether these pores are functional channels. Based on the crystal structure of lysenin, it is speculated that, in the prepore state, the N-terminus of lysenin partially spans the membrane through its specific binding to SM in the outer leaflet of the bilayer (9). This partial insertion might induce a conformational change in the core of lysenin, leading to pore formation. As an alternative, the C-terminus might bind the membrane first whereas the N-terminus is tilted upwards in the hexameric prepore state (see Fig. S3). Subsequent insertion of the N-terminus might induce the conversion from prepore to pore state.

In addition to the ring-like oligomers, incomplete arc-shaped oligomers were occasionally detected (Fig. 1 *A*, indicated by *arrows*). The average height difference between ring-like and arc-shaped oligomers was ~0.25 nm, negligible compared to the height distribution shown in Fig. 1 *C*. The presence of lower arc-shaped oligomers denotes that extended insertion into the membrane can occur before completion of oligomerization (28). Nevertheless, the growth of oligomers seems to be faster than insertion, because the majority of lysenin oligomers are complete rings of similar diameter and height.

The band-pass filtered image revealed bridge-like structures between neighboring oligomers (Fig. 1 *D*, indicated by *arrows*). Similar structural features have also been observed in oligomers of other toxins, such as VacA, sticholysin II, and cholera toxin (3,4,29). These bridge-like structures have not been characterized yet. It is speculated that they may be formed by either the N-terminus or the C-terminus of the toxin. De Colibus et al. (9) suggested that the N-terminus of lysenin partially penetrates the membrane and is not subjected to reconfiguration in the prepore state, leaving the three two-stranded hairpins in the C-terminus as potential candidates to form the bridge-like structures. As of this writing, the possibility that the observed structures were caused by the AFM tip during imaging cannot be completely ruled out.

Reorganization of lysenin during assembling

We then followed the time course of the assembling of lysenin on the SM/chol bilayer in situ at a scan rate of 3.3 frames/s over a scan area of 250 × 250 nm (see Movie S1 and Fig. S4 in the Supporting Material). Initially, there were only a few unfused vesicles (see Fig. S4 *A*, marked by *asterisk*) on the membrane and lysenin monomers, moving too fast to be localized under our experimental conditions. The unfused vesicles were generally observed in addition to the fused lipid bilayer in the acquired images. After 2 min, oligomer-like assemblies of lysenin slowly started to appear. A direct comparison of these assemblies with the oligomers in Fig. 1 *A* is difficult due to their unclear size and shape. Consequently, the term "cluster" will be used instead of "oligomer" to describe and discuss the in-situ observations. In this context, clusters might be the intermediate assemblies of lysenin (dimer, trimer, tetramer, open-ring, etc.) or rapidly associating/dissociating oligomers. With the increasing cluster number on the membrane, an hcp structure was formed in <5 min.

Next, we tracked the assembling of lysenin on the SM/chol bilayer at a larger scan area of 400 × 300 nm and a

lower scan rate of 0.5 frames/s (see Movie S2 and Fig. S5). In selected images of this movie (Fig. 2 *A*) it is possible to see the overall change in the packing of the lysenin clusters and the change in the growth direction of the cluster arrays. In addition to the round-shaped clusters, rapidly moving irregular-shaped monomers/clusters can be observed. During the course of the reaction, most of the round-shaped clusters assembled into an hcp structure. Aside from lysenin assembling on the SM/chol bilayer, lysenin also adsorbed directly on mica, the lowest area in Fig. 2 *A*. The particle radius of the membrane-bound lysenin after full coverage (36 s) was found to be very similar to hcp oligomers (see Fig. S6, *A* and *C*). In contrast, the size analysis for lysenin on mica yielded a much broader distribution, indicating

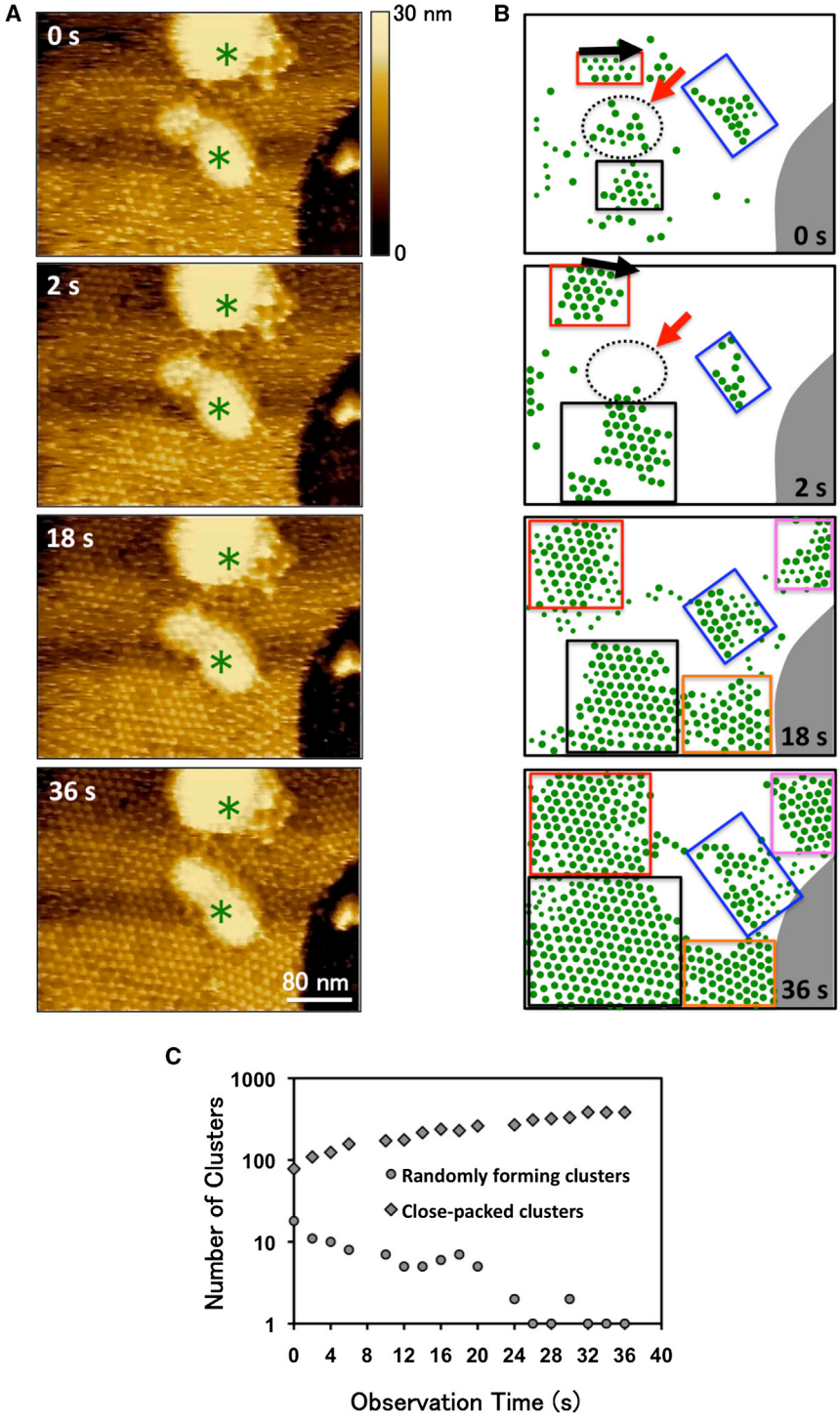

FIGURE 2 *(A)* Time-lapse AFM images of lysenin clusters forming the hcp structure on SM/chol (1:1) bilayer. Lysenin was injected into PBS and assembling of lysenin on SM/chol (1:1) bilayer was followed at a scan rate of 0.5 frames/s. Time "0 s" is the starting time of the observation period. Asterisks indicate the unfused vesicles. *(B)* Schematic illustration of the AFM images in panel *A* showing the growth of domains of lysenin clusters in different regions. Each lysenin cluster is depicted in green. Small dots represent irregular shaped clusters, perhaps the intermediates, and large dots show round shaped, presumably the final oligomers. Black and blue frames indicate the continuously growing and unstable-disordered domains, respectively. Red, orange and pink frames correspond to the unstable-ordered domains. In black-framed region, the initially formed clusters in hcp structure are stable and new clusters bind to this domain, enlarging the stable hcp structure. In blue-framed region, clusters show a dynamic behaviour and an hcp structure does not form. In red, orange and pink-framed regions, clusters might associate/dissociate or diffuse laterally to arrange into an hcp structure. *(C)* Change in the number of randomly forming and close-packed clusters within the observation time.

that lysenin exists on mica as a mixture of monomers and irregular-shaped aggregates (see Fig. S6, *B* and *C*). The difference in particle size distribution between lysenin aggregates on mica and lysenin clusters on the membrane strongly suggests that lysenin cannot form oligomers on membrane-free surface as described previously by Yamaji-Hasegawa et al. (8). For a better understanding of the formation of the hcp structure, each round-shaped cluster is depicted as a green dot in Fig. 2 *B*. The green dots were placed manually on the clusters that could be easily recognized by eye. The frames in different colors highlight the growth of the domains of lysenin clusters. Assembling of lysenin on the SM/chol bilayer exhibits the following distinctive features:

Random formation of clusters

In the initial stages of assembling (0 s in Fig. 2 *B*), either individual or arrays of clusters formed randomly in different regions of the membrane surface. The randomly forming clusters were more dynamic than the close-packed clusters. Most of the randomly forming clusters dissociated or diffused along the membrane. The time-dependent change in the number of randomly forming and close-packed clusters is shown in Fig. 2 *C*. As the number of close-packed clusters increased by time, randomly forming clusters gradually diminished. This suggests that, at first, lysenin forms individual clusters, which in turn diffuse along the membrane surface to arrange into an hcp structure.

Cooperative association/dissociation of clusters

Within a few seconds, while new clusters formed, both filling the gaps within the arrays and forming new arrays, some of the existing clusters either dissociated or diffused along the membrane surface (e.g., the areas indicated by the *red arrow* in Fig. 2 *B* at 0 and 2 s).

Change in the direction of cluster arrays

In some of the regions, the direction of the cluster arrays changed. The clusters that formed within the top-left frame in red at 2 s were aligned in a different direction than those which formed at 0 s (Fig. 2 *B*). The directions of the cluster arrays within the red frame at 0 s and 2 s are indicated by the black arrows.

Similar packing density of clusters in different domains

A small domain of stable lysenin clusters formed within the black-framed region at 0 s and continued growing (Fig. 2 *B*). In the red, orange, and pink-framed regions, lysenin clusters initially formed unstable domains in which the clusters either dissociated/reassociated or changed their positions. We named these domains "unstable-ordered" due to their dynamic behavior during the formation of the hcp structure. The clusters in the blue-framed region were both unstable and disordered. Ultimately, the domains in different regions combined and the membrane surface was fully covered with a stable hcp assembly of lysenin. The overlay of images at 0, 2, 18, and 36 s at an opacity of 50% shows the change in the position of clusters (Fig. 3 *A*). The lower contrast of the overlay compared to the image at 36 s (Fig. 2 *A*) indicates the change in the position of clusters before the formation of the stable hcp assembly. The high-contrast domains in the overlay imply the reduced dynamics of clusters during assembling. The domains of lysenin clusters within the black, red, and orange frames were analyzed to find the average

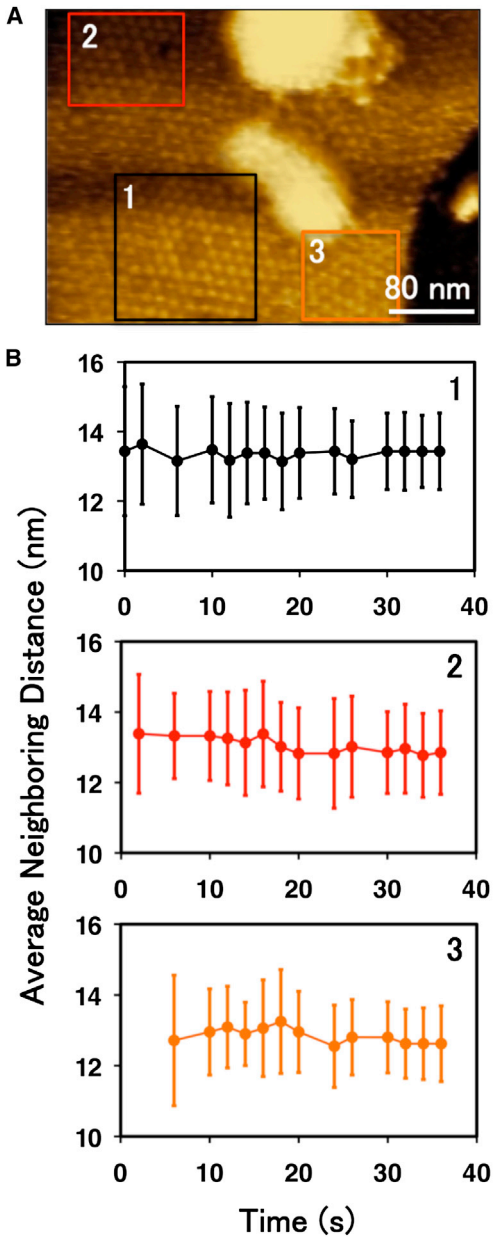

FIGURE 3 Change in the packing density of lysenin clusters. (*A*) Overlay of images at 0, 2, 18, and 36 s at an opacity of 50%. (*B*) Average neighboring distance as a function of time for the continuously growing region 1, and the unstable-ordered regions 2 and 3. (Colors in panel *B* correspond to the regions in *black*, *red*, and *orange* frames in panel *A*.)

neighboring distance between clusters. The change in the average distance between two neighboring clusters calculated for three different regions on the membrane surface is shown together with the standard deviation as a function of time in Fig. 3 *B*. The analyzed regions are indicated in Fig. S5. The average neighboring distance could be calculated only for the domains of lysenin clusters showing an ordered arrangement. The average neighboring distance for these ordered domains did not greatly change in either space or time. There was a decrease in the standard deviation as the ordered domains grew larger. The higher standard deviation at the initial period of assembling is due to the randomly forming clusters around those showing an ordered arrangement. Most of the lysenin clusters formed rapidly reversible/irreversible arrays or domains with the same average neighboring distance instead of random distribution on the membrane even during the initial period of assembling.

The arrangement of lysenin clusters into an hcp structure seems to be dependent on the liquid-ordered phase of the SM/chol bilayer (30). The same process was also followed on pure SM bilayer; however, we did not observe the formation of an hcp structure (see Movie S3; scan rate: 1 frame/s, scan area: 500 × 500 nm, real scan time: 3 min 38 s). In contrast to SM/chol, SM membrane exhibits a gel-like behavior at room temperature (31). Previously, we reported that the binding of lysenin to SM and SM/chol membranes was similar; however, oligomerization was facilitated by the presence of chol due to the change in the membrane fluidity (14). Therefore, in our study we suggest that the observed difference in the assembling of lysenin on SM and SM/chol membranes is due to the difference in the membrane fluidity, which affects oligomerization and hence formation of a well-ordered structure.

Subsecond association/dissociation of lysenin clusters

The association and dissociation of lysenin clusters from the edge of a domain of close-packed clusters was followed at a higher magnification (85 × 40 nm) and a higher scan rate (6.7 frames/s) for a more careful examination of the dynamics of clusters during assembling into an hcp structure (Fig. 4 *A* and see Movie S4). The lysenin clusters at the domain edge are depicted as green dots (Fig. 4 *B*). The cluster, indicated by the white arrow at 0 s, disappeared at 0.15 s. This might be due to the dissociation of the cluster into monomers, dimers, etc., or the detachment of the cluster from the domain. Monomers, intermediates, and free clusters appear as spikes in the images and cannot be clearly distinguished due to their rapid diffusion along the membrane surface. The neighboring clusters (indicated by *red arrows*) also started to dissociate at 0.3 s. However, at 0.45 s simultaneous reassociation of three neighboring clusters occurred. The cooperative association/dissociation of clusters is marked with white dashed-line rectangles. The dissociation and reassociation of the cluster

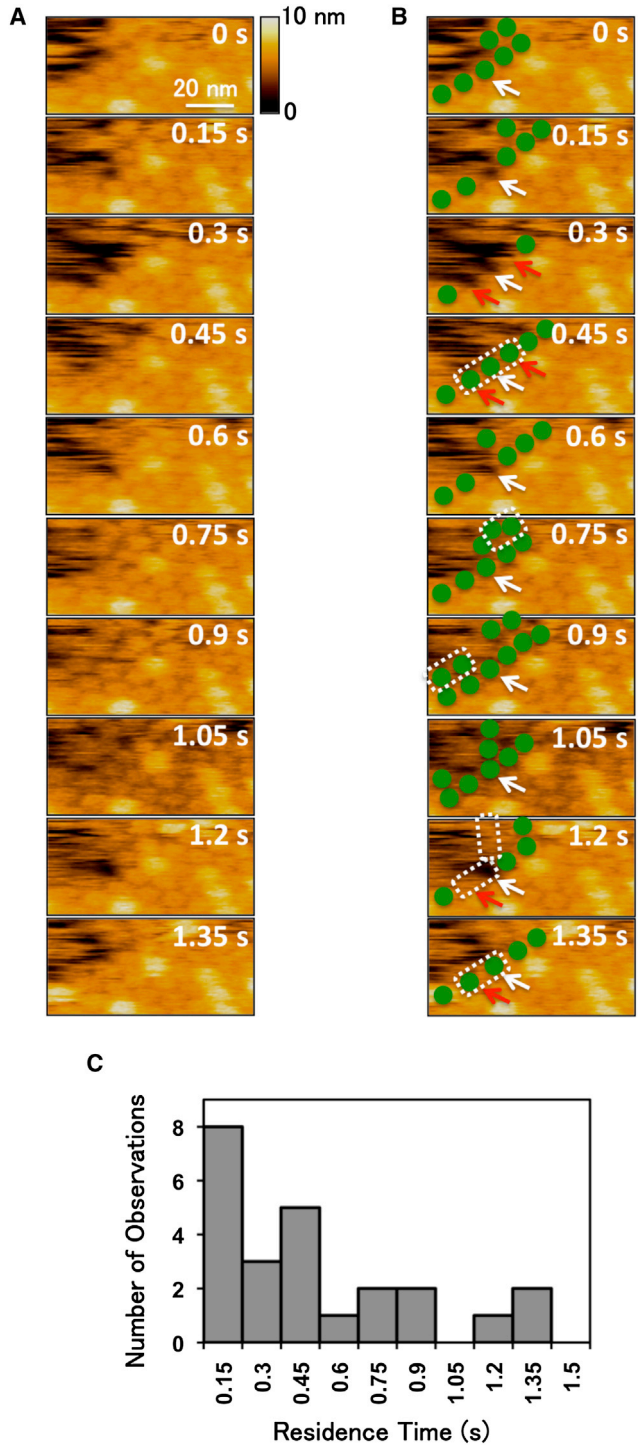

FIGURE 4 (*A*) AFM images showing the dynamics of lysenin clusters on SM/chol (1:1) bilayer. Association/dissociation of clusters at the domain edge was followed at a scan rate of 6.7 frames/s. (*B*) AFM images in panel *A* with the schematic outline of the association/dissociation of clusters at the domain edge. (*C*) Histogram showing the number of observations for different residence times before dissociation.

at the location indicated by the white arrow occurred at 0.15, 0.6, and 1.2 s, and 0.45, 0.75, and 1.35 s, respectively. The residence time before dissociation of the clusters at the

domain edge was analyzed (Fig. 4 *C*). In most cases, clusters dissociated within 0.15 s after binding to the domain. The average residence time was found to be ~0.45 s. This is comparable to the residence times of bacteriorhodopsin trimers and aquaporin tetramers, previously studied by HS-AFM (16,32). In a report by Yamashita et al. (16), examination of the effect of tip velocity on the lifetime of the trimers of bacteriorhodopsin revealed that the dynamics of trimers was not dependent on tip velocity. Hence, we think that the association/dissociation of lysenin oligomers was not affected by the tip. In contrast to the clusters at the edge of the domain, those within the hexagonal structure were relatively stable. The instability of the clusters at the domain edge may result from the smaller number of interaction sites. The clusters within the hexagonal structure, which seem to be the oligomers, are linked to each other through six interaction sites, rendering them more stable than those at the edges. Another reason might be the conformational energy barrier between lysenin molecules in adjacent clusters (33), leading to the breakage of the intermolecular interaction between the clusters.

Lysenin clusters did not always follow the same reorganization pathway (see Fig. S7). After the binding of new clusters, some of the clusters within the same domain dissociated at random locations, leaving arrays of clusters aligned in different directions. This implies that the organization of lysenin clusters was not unidirectional before the formation of the stable hcp structure.

Subsecond changes in cluster height

Besides monitoring the fast association/dissociation of lysenin clusters, the change in cluster height was also monitored. In Fig. 5, *A–C*, the height change of a cluster within an hcp structure is shown for a scan area of 85 × 40 nm and a scan rate of 6.7 frames/s. The height profiles along the yellow line, marked at 0 s in Fig. 5 *B*, are shown in Fig. 5 *C*. The cluster indicated by the arrow in Fig. 5 *B* dissociated at 0.15 s, leaving a depression of 1.4 nm, and reassociated at 0.3 s at the same height with the adjacent cluster along the yellow line. After 0.3 s, the cluster dissociation/reassociation took place with an increase in height. The sequential pattern of changes was as follows: there was an increase of 2.8 nm in the cluster height at 0.75 s, followed by a diffusion of the cluster along the membrane surface, leaving a depression of 2.5 nm in the hcp structure at 0.9 s, and finally a filling of the gap, along with a decrease in its height at 1.5 s. The diffusion or dissociation of clusters is an indication of their instability. The same cluster underwent similar changes after an additional dissociation at 4.65 s, followed by the appearance of a brighter oligomer at 4.8 s and a decrease in its height within a time interval of $<$0.45 s. The depressions observed at 0.15, 0.9, and 4.65 s were of different heights. This might be due to the incomplete dissociation of the cluster when the image was captured. Because lysenin is a water-soluble protein and forms oligomers only in the presence of SM, the binding of lysenin to the SM-bound lysenin and its oligomerization on the first layer seems to be unlikely. Thus, the observation of the (brighter) taller oligomers just before the dissociation and after association supports the possibility of conformational changes in lysenin rather than multilayer formation. Considering the size of lysenin, which is ~10 nm in length, a change in its height up to 3 nm seems to be resulting from the reversible partial insertion of clusters into the membrane by vertical collapse. Therefore, the height change might be an indication of the transition from prepore to pore. However, we do not know the penetration depth of the clusters into the membrane before the formation of a stable hcp structure. The transition of a complete pore to prepore seems unlikely. Therefore, partial and weak insertion of clusters into the membrane is more plausible. After the completion of a stable hcp structure, some taller oligomers (see Fig. S8, indicated by *arrows*) showed a decrease in height whereas most oligomers kept the same conformation. We did not observe any increase in the height of lower oligomers within the stable hcp structure.

CONCLUSIONS

This work demonstrates the assembling of lysenin on an SM-containing membrane. The high-speed AFM images revealed the dynamics of the association of lysenin clusters into an hcp structure. Initially, both individual and small domains of lysenin clusters formed randomly at different locations on the membrane. Although some of these domains grew continuously, most of them reorganized by subsecond dissociation/reassociation of the clusters. In addition to reorganization of the clusters, the changes in the cluster height could also be followed. The subsequent increases and decreases in the cluster height can be an indication of the conformational changes of lysenin, resulting in its vertical collapse and membrane insertion. After the membrane surface had been fully covered with close-packed clusters, the hcp structure stabilized. The liquid-ordered behavior of the SM/chol membrane facilitates the diffusion of the clusters along the membrane and the formation of the hcp structure. The similar size of the clusters and their occasionally observed porous structure imply the formation of rapidly reversible/irreversible oligomers of lysenin during its assembling on SM/chol bilayer. Our results suggest that the assembling of lysenin on the membrane into an hcp structure is dependent on the rapid association/dissociation and diffusion of lysenin oligomers.

SM-rich lipid clusters do not randomly distribute in cell membranes. Instead, they form domains whose radius is 60–80 nm on the outer leaflet of the plasma membrane (12). Lysenin-treated red blood cells produce globular protrusions rich in lysenin as revealed by immuno-electron

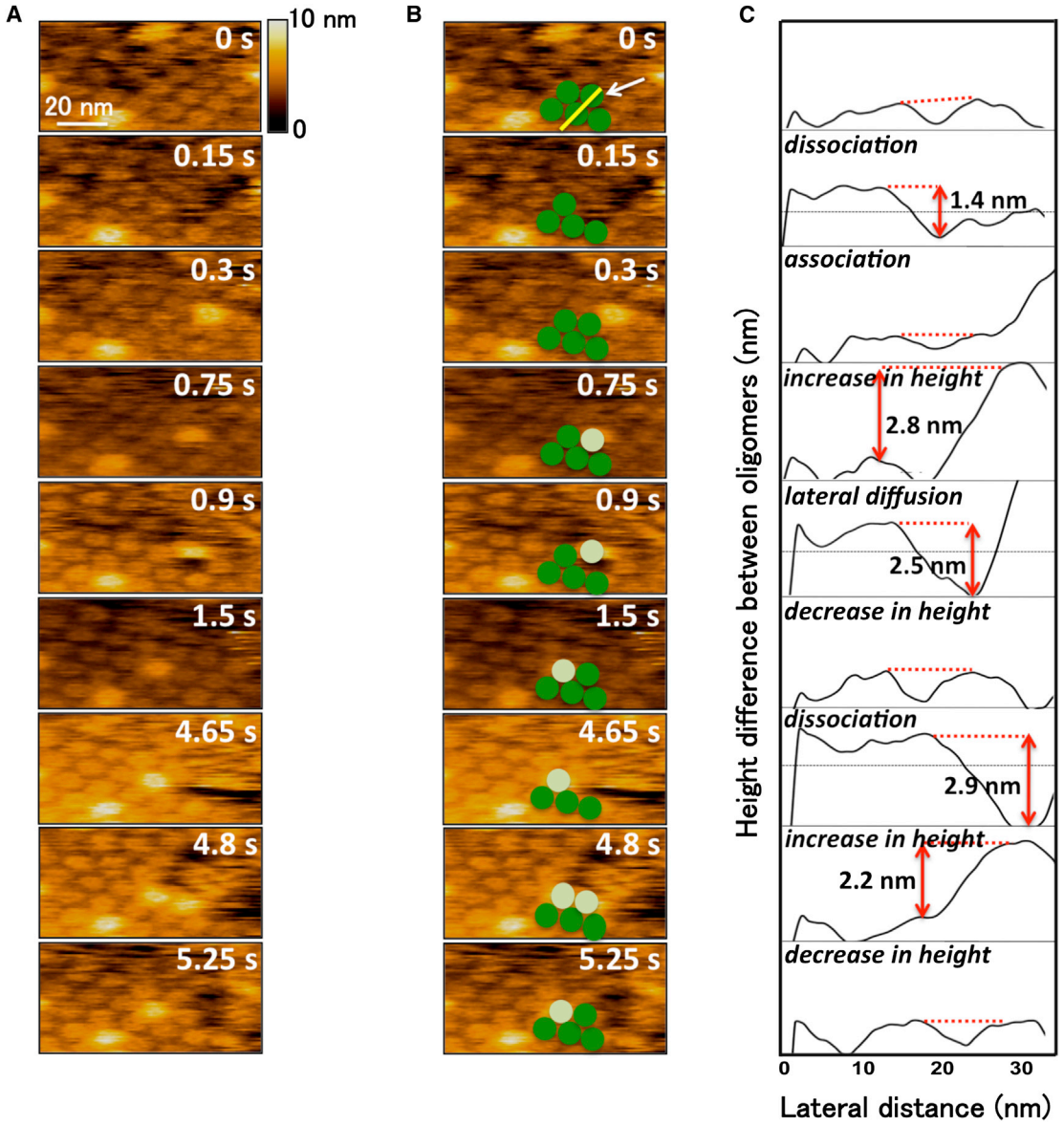

FIGURE 5 (*A*) AFM images showing the height change for a particular lysenin cluster on SM/chol (1:1) bilayer. The height change and the association/dissociation of the cluster were followed at a scan rate of 6.7 frames/s. (*B*) AFM images in panel *A* with the schematic outline of the association/dissociation of the cluster within the hexagonal structure and the time-dependent change in the cluster height. (*Pale green*) Taller oligomers. (*C*) Height profiles (along the *yellow line*) in panel *B*. (*Dashed line*) Baseline at 0 s.

microscopy (8). These protrusions contain aggregates of round-shaped structures whose diameter is 10–15 nm (8). Although the pores are not clearly observed, it is speculated that these aggregates correspond to the hcp structure. Formation of the hcp structure is advantageous for pore formation because hcp stabilizes the pores.

SUPPORTING MATERIAL

Eight figures and four movies are available at http://www.biophysj.org/biophysj/supplemental/S0006-3495(13)00878-3.

The authors thank Dr. N. Kotani and Ms. A. Kanegami for performing some of the high-speed AFM experiments at RIBM (Tsukuba, Japan).

This work was supported by the Lipid Dynamics Program of RIKEN and Grants-in-Aid for Scientific Research Nos. 22390018 and 25293015 (to T.K.) from the Ministry of Education, Culture, Sports, Science and Technology of Japan.

REFERENCES

1. Iacovache, I., M. Bischofberger, and F. G. van der Goot. 2010. Structure and assembly of pore-forming proteins. *Curr. Opin. Struct. Biol.* 20:241–246.
2. Czajkowsky, D. M., S. Sheng, and Z. Shao. 1998. Staphylococcal α-hemolysin can form hexamers in phospholipid bilayers. *J. Mol. Biol.* 276:325–330.
3. Czajkowsky, D. M., H. Iwamoto, …, Z. Shao. 1999. The vacuolating toxin from *Helicobacter pylori* forms hexameric pores

in lipid bilayers at low pH. *Proc. Natl. Acad. Sci. USA*. 96:2001–2006.

4. Mancheño, J. M., J. Martín-Benito, …, L. Vázquez. 2006. A complementary microscopy analysis of Sticholysin II crystals on lipid films: atomic force and transmission electron characterizations. *Biophys. Chem*. 119:219–223.
5. Shakor, A. B., E. A. Czurylo, and A. Sobota. 2003. Lysenin, a unique sphingomyelin-binding protein. *FEBS Lett*. 542:1–6.
6. Shogomori, H., and T. Kobayashi. 2008. Lysenin: a sphingomyelin specific pore-forming toxin. *Biochim. Biophys. Acta*. 1780:612–618.
7. Yamaji, A., Y. Sekizawa, …, M. Umeda. 1998. Lysenin, a novel sphingomyelin-specific binding protein. *J. Biol. Chem*. 273:5300–5306.
8. Yamaji-Hasegawa, A., A. Makino, …, T. Kobayashi. 2003. Oligomerization and pore formation of a sphingomyelin-specific toxin, lysenin. *J. Biol. Chem*. 278:22762–22770.
9. De Colibus, L., A. F. Sonnen, …, R. J. Gilbert. 2012. Structures of lysenin reveal a shared evolutionary origin for pore-forming proteins and its mode of sphingomyelin recognition. *Structure*. 20:1498–1507.
10. Hannun, Y. A., and L. M. Obeid. 2008. Principles of bioactive lipid signaling: lessons from sphingolipids. *Nat. Rev. Mol. Cell Biol*. 9:139–150.
11. Lingwood, D., and K. Simons. 2010. Lipid rafts as a membrane-organizing principle. *Science.* 327:46–50.
12. Kiyokawa, E., T. Baba, …, T. Kobayashi. 2005. Spatial and functional heterogeneity of sphingolipid-rich membrane domains. *J. Biol. Chem*. 280:24072–24084.
13. Abe, M., A. Makino, …, T. Kobayashi. 2012. A role for sphingomyelin-rich lipid domains in the accumulation of phosphatidylinositol-4,5-bisphosphate to the cleavage furrow during cytokinesis. *Mol. Cell. Biol*. 32:1396–1407.
14. Ishitsuka, R., and T. Kobayashi. 2007. Cholesterol and lipid/protein ratio control the oligomerization of a sphingomyelin-specific toxin, lysenin. *Biochemistry.* 46:1495–1502.
15. Ando, T., N. Kodera, …, A. Toda. 2001. A high-speed atomic force microscope for studying biological macromolecules. *Proc. Natl. Acad. Sci. USA*. 98:12468–12472.
16. Yamashita, H., K. Voïtchovsky, …, T. Ando. 2009. Dynamics of bacteriorhodopsin 2D crystal observed by high-speed atomic force microscopy. *J. Struct. Biol*. 167:153–158.
17. Casuso, I., P. Sens, …, S. Scheuring. 2010. Experimental evidence for membrane-mediated protein-protein interaction. *Biophys. J*. 99: L47–L49.
18. Casuso, I., J. Khao, …, S. Scheuring. 2012. Characterization of the motion of membrane proteins using high-speed atomic force microscopy. *Nat. Nanotechnol*. 7:525–529.
19. Uchihashi, T., N. Kodera, and T. Ando. 2012. Guide to video recording of structure dynamics and dynamic processes of proteins by high-speed atomic force microscopy. *Nat. Protoc*. 7:1193–1206.
20. Roy, A., A. Kucukural, and Y. Zhang. 2010. I-TASSER: a unified platform for automated protein structure and function prediction. *Nat. Protoc*. 5:725–738.
21. Zhang, Y. 2008. I-TASSER server for protein 3D structure prediction. *BMC Bioinformatics.* 9:40.
22. Roy, A., J. Yang, and Y. Zhang. 2012. COFACTOR: an accurate comparative algorithm for structure-based protein function annotation. *Nucleic Acids Res*. 40(Web Server issue):W471–W477.
23. Anandakrishnan, R., B. Aguilar, and A. V. Onufriev. 2012. H^{++} 3.0: automating pK prediction and the preparation of biomolecular structures for atomistic molecular modeling and simulations. *Nucleic Acids Res*. 40(Web Server issue):W537–W541.
24. MacKerell, Jr., A. D., M. Feig, and C. L. Brooks, 3rd. 2004. Extending the treatment of backbone energetics in protein force fields: limitations of gas-phase quantum mechanics in reproducing protein conformational distributions in molecular dynamics simulations. *J. Comput. Chem.* 25:1400–1415.
25. Phillips, J. C., R. Braun, …, K. Schulten. 2005. Scalable molecular dynamics with NAMD. *J. Comput. Chem.* 26:1781–1802.
26. Humphrey, W., A. Dalke, and K. Schulten. 1996. VMD: visual molecular dynamics. *J. Mol. Graph.* 14:27–38.
27. Czajkowsky, D. M., E. M. Hotze, …, R. K. Tweten. 2004. Vertical collapse of a cytolysin prepore moves its transmembrane β-hairpins to the membrane. *EMBO J*. 23:3206–3215.
28. Gilbert, R. J., M. Mikelj, …, G. Anderluh. 2013. Effects of MACPF/CDC proteins on lipid membranes. *Cell. Mol. Life Sci*. 70:2083–2098.
29. Mou, J., J. Yang, and Z. Shao. 1995. Atomic force microscopy of cholera toxin B-oligomers bound to bilayers of biologically relevant lipids. *J. Mol. Biol*. 248:507–512.
30. Ramstedt, B., and J. P. Slotte. 2002. Membrane properties of sphingomyelins. *FEBS Lett*. 531:33–37.
31. Janosi, L., and A. Gorfe. 2010. Importance of the sphingosine base double-bond geometry for the structural and thermodynamic properties of sphingomyelin bilayers. *Biophys. J*. 99:2957–2966.
32. Colom, A., I. Casuso, …, S. Scheuring. 2012. High-speed atomic force microscopy: cooperative adhesion and dynamic equilibrium of junctional microdomain membrane proteins. *J. Mol. Biol*. 423:249–256.
33. Lomakin, A., N. Asherie, and G. B. Benedek. 1999. Aeolotopic interactions of globular proteins. *Proc. Natl. Acad. Sci. USA*. 96:9465–9468.